

# The Mechanism of Assembly of *Acanthamoeba* Myosin-II Minifilaments: Minifilaments Assemble by Three Successive Dimerization Steps

John H. Sinard, Walter F. Stafford,\* and Thomas D. Pollard

The Department of Cell Biology and Anatomy, The Johns Hopkins University School of Medicine, Baltimore, Maryland 21205; and \*The Department of Muscle Research, The Boston Biomedical Research Institute, and The Department of Neurology, Harvard Medical School, Boston, Massachusetts 02114

**Abstract.** We used 90° light scattering, analytical ultracentrifugation, and electron microscopy to deduce that *Acanthamoeba* myosin-II minifilaments, composed of eight molecules each, assemble by a novel mechanism consisting of three successive dimerization steps rather than by the addition of monomers or parallel dimers to a nucleus. Above 200 mM KCl, *Acanthamoeba* myosin-II is monomeric. At low ionic strength (<100 mM KCl), myosin-II polymerizes into bipolar minifilaments. Between 100 and 200 mM KCl, plots of light scattering vs. myosin concentration all extrapolate to the origin but have slopes which decrease with increasing KCl. This indicates that structures intermediate in size between monomers and full length minifilaments are formed, and that the critical concentrations for assembly of these structures is very low. Analytical ultracentrifugation has confirmed that

intermediate structures exist at these salt concentrations, and that they are in rapid equilibrium with each other. We believe these structures represent assembly intermediates and have used equilibrium analytical ultracentrifugation and electron microscopy to identify them. Polymerization begins with the formation of antiparallel dimers, with the two tails overlapping by ~15 nm. Two antiparallel dimers then associate with a 15-nm stagger to form an antiparallel tetramer. Finally, two tetramers associate with a 30-nm stagger to form the completed minifilament. At very low ionic strengths, the last step in the assembly mechanism is largely reversed and antiparallel tetramers are the predominant species. Alkaline pH, which can also induce minifilament disassembly, produces the same assembly intermediates as are found for salt induced disassembly.

**A**LL known two-headed, conventional myosins (referred to as myosins-II, to distinguish them from the single-headed myosin I; see Korn and Hammer, 1988, for terminology) can assemble into bipolar filaments at low ionic strength, and, in fact, this ability has become a fundamental part of the working definition of this type of myosin. These myosins have two globular heads at the end of an alpha-helical coiled-coil tail, the length of which varies from species to species. The structures of the myosin-II filaments vary widely and depend not only on the source of the myosin but also upon the ionic strength, pH, divalent cation composition, and the presence or absence of copolymerizing proteins. For example, skeletal muscle myosin forms thick, heterogeneous filaments 12  $\mu\text{m}$  long at pH 7.0, but forms thinner, more homogeneous bipolar filaments 630 nm long at pH 8.0 (Josephs and Harrington, 1966), and forms 300-nm-long bipolar minifilaments composed of ~16 myosin molecules each in 10 mM Tris/citrate buffer, pH 8.0, with no KCl (Reisler et al., 1980). Homogeneous, pH 8.0, synthetic filaments can be grown from minifilaments by the addition of KCl (Reisler et al., 1982), suggesting that the minifilament may form part of the bare zone containing core of the myosin filament and thus nucleate myosin filament assembly.

Myosins from vertebrate nonmuscle cells (Niedermaier and Pollard, 1975), *Acanthamoeba* (Pollard et al., 1978), vertebrate smooth muscle (Trybus and Lowey, 1985), and *Dictyostelium* (Kuczmarski et al., 1988) also form small bipolar minifilaments, although the required conditions vary. Smooth muscle myosin minifilaments form under conditions similar to those used to make skeletal muscle myosin minifilaments (Trybus and Lowey, 1985), but upon addition of KCl, these minifilaments grow to form "side polar" rather than bipolar filaments. The side polar filaments have bare zones at either end and heads with uniform but opposite orientation on the two sides (Trybus and Lowey, 1987). *Acanthamoeba* myosin-II minifilaments form over a KCl concentration range between 10 and 100 mM (Sinard and Pollard, 1989), and no known conditions induce these minifilaments to grow longer. On the other hand, divalent cations or acidic pH cause the lateral aggregation of myosin-II minifilaments into larger structures termed "thick filaments" (Pollard, 1982; Sinard and Pollard, 1989). *Dictyostelium* myosin-II in 40 mM KCl forms small bipolar structures very similar to minifilaments (Kuczmarski et al., 1988). Inclusion of  $\text{Mg}^{++}$  produces larger polymers resembling the synthetic filaments of skeletal muscle myosin or the thicker filaments of *Acanthamoeba* myosin-II (Clarke

and Spudich, 1974; Stewart and Spudich, 1979; Kuczumarski and Spudich, 1980; Kuczumarski et al., 1987). Therefore, the ability to form minifilaments seems to be a universal property of myosins-II.

Most of the previous work on the mechanism of assembly of myosin filaments has been done on pH 8.0 synthetic filaments of skeletal muscle myosin-II. Davis and co-workers (for review, see Davis, 1988), using turbidity as an assay and pressure jump to initiate polymerization or depolymerization, identified a parallel dimer with a 44-nm axial stagger as the functional assembly unit for synthetic filament elongation and measured the rate constants for subunit association and dissociation at the filament ends. However, as of yet, little direct work has been done on the mechanism of minifilament formation or the nucleation of larger filaments.

*Acanthamoeba* myosin-II is an ideal system for studying the assembly of minifilaments since they do not elongate into larger structures. In the previous paper, we used 90° light scattering and electron microscopy to quantitate factors affecting the assembly of *Acanthamoeba* myosin-II (Sinard and Pollard, 1989). Here, we provide a variety of data that has revealed the mechanism of myosin-II minifilament assembly. First, we characterize the structure of the completed minifilament by electron microscopy and analytical ultracentrifugation. Secondly, we use light scattering, computer modeling, and velocity sedimentation to establish the presence of assembly intermediates under certain ionic conditions. Finally, we use electron microscopy and equilibrium ultracentrifugation to determine the structures of the intermediates and the sequence of association of the monomers through the intermediates into fully formed minifilaments. In contrast to the elongation of synthetic filaments which occurs by the addition of parallel dimers to both ends of the growing filament, *Acanthamoeba* myosin-II minifilaments form by the stepwise dimerization of increasingly higher ordered structures. The initial event is the formation of an antiparallel dimer, which subsequently dimerizes to form an antiparallel tetramer. Two such antiparallel tetramers then dimerize to form the completed octamer.

## Materials and Methods

*Acanthamoeba* myosin-II was prepared and dephosphorylated as described (Sinard and Pollard, 1989). Dephosphorylated myosin-II containing 0.6–1.2 phosphates per molecule was used in all of the experiments described here. The 90° light scattering assay was performed in a fluorescence spectrophotometer at a wavelength of 365 nm (Sinard and Pollard, 1989).

### Electron Microscopy

Samples for rotary shadowing were prepared at twice the desired final ionic strength and then diluted with an equal volume of glycerol. After equilibration (1–2 min), they were sprayed onto freshly cleaved mica. Shadowing, negative staining, and electron microscopy were done as described (Sinard and Pollard, 1989).

### Analytical Ultracentrifugation

Velocity sedimentation runs were performed at 20°C in an ultracentrifuge (model E; Beckman Instruments, Inc., Palo Alto, CA) equipped with a UV photoelectric scanner at a wavelength of 280 nm. The output from the scanner was digitized using an analog-to-digital board (model NB-MIO-16H-9; National Instrument Co., Inc., Baltimore, MD) in an Apple Computer Corporation Macintosh-II microcomputer. Gradient curves ( $dc/dr$  vs.  $r$ ) were obtained from the optical density profiles by numerically smoothing and differentiating the digitized scans using standard numerical procedures (Hil-

debrand, 1956). These curves were converted to apparent sedimentation coefficient distributions ( $g^*(s)$  vs.  $s$ ) using the Bridgman (1942) equation by the following manipulations: on the  $x$ -axis, the radius value was converted to a sedimentation coefficient by taking into account the time and speed of centrifugation; this sedimentation coefficient was then corrected for the buffer used, which routinely contained 5% sucrose, to the appropriate value in water at 20°C. On the  $y$ -axis, the  $dc/dr$  values were multiplied by  $dr/dS$  and corrected for radial dilution. This made the  $x$ -axis time and speed independent and allowed samplings at multiple times to be averaged at each value of  $s$  to increase the signal to noise ratio. All sedimentation coefficients referred to in the text are corrected to water at 20°C. Sedimentation equilibrium runs were carried out at 2–4°C over a range of initial loading concentrations and rotor speeds. Blank runs, used to make optical background corrections, were performed for every experiment at the same temperature and speed as the run (Yphantis, 1964; Roark and Yphantis, 1969; Ansevin et al., 1970). The reader is referred to the review by Teller (1973) for a more general description of the method. The equilibrium runs were performed on an analytical ultracentrifuge (model E; Beckman Instruments, Inc.) equipped with Rayleigh optics and an externally adjustable Rayleigh mask assembly (Stafford, 1978). A polarized helium-neon laser light source was used in continuous mode. Sapphire cell windows were used and the camera was focused at the 2/3 plane of the cell (Yphantis, 1964; Richards et al., 1971, 1972). Externally loading six-channel, 12-mm centerpieces were used (Ansevin et al., 1970). Rayleigh interferograms were taken on Kodak Technical Pan film 2415 on estar-AH base (cat. no. 1299916). The Rayleigh photographs were read at 25- $\mu$ m intervals using an automated plate reader controlled by an 8080A microprocessor system using an arrangement based on a Reticon photodiode array. Fringe displacements were obtained using the Fourier analysis method adapted from DeRosier et al. (1972) using code written in assembly language for the 8080A system. Fringe displacement data were analyzed on an Apple Macintosh-II microcomputer using the techniques and computer programs described (Roark and Yphantis, 1969; Teller, 1973; Margossian and Stafford, 1982). A value of 0.728 cc/g was used for the partial specific volume, calculated from the amino acid composition of myosin-II (Pollard et al., 1978). The molecular weight averages obtained were used to construct so-called "two species" plots (Sophianopoulos and Van Holde, 1964; Roark and Yphantis, 1969). For a two-species system, a plot of  $M_z$  vs.  $1/M_w$  (or  $M_w$  vs.  $1/M_n$ ) will be a straight line with slope  $(-M_1M_2)$  and intercept  $(M_1 + M_2)$ , where  $M_1$  and  $M_2$  are the molecular weights of species 1 and 2, respectively, and  $M_n$ ,  $M_w$ , and  $M_z$  are the number, weight, and z-average molecular weights, respectively. The two-species curve will intersect a hyperbola (defined by  $M_n = M_w = M_z$ ) at  $M_1$  and  $M_2$  (see, for example, Fig. 5). The hyperbola represents the locus of all possible single species systems. The plot for thermodynamically ideal systems composed of more than two species will be curved upward and intersect the hyperbola at the lower end at the molecular weight of the smallest species present and, at the higher end, at the molecular weight of the largest species. Lack of curvature over limited ranges of the plot is an indication that only two species are present in significant amounts over that range of concentration. For a multi species system the data must plot within the boundaries specified by a polygon whose vertices are the points on the hyperbola corresponding to the molecular weights of the species present in the system. Therefore, these plots can be used to rule out some possible stoichiometries as well as to obtain the molecular weights of the largest and smallest species visible in the solution column.

### Computer Modeling of Light Scattering

The computer modeling of the light scattering data was performed on an Apple-II Plus computer. The program, written in BASIC, required input of species size (no. of monomers per polymer), equilibrium constants for each reaction, and scattering coefficients for each of the species. It performed multiple iterations on all of the reaction equations until the total flux of monomers between species for a single iteration was  $<1$  nM. Net light scattering was calculated as the sum of the scattering coefficient for each species multiplied by its concentration. Total light scattering was plotted as a function of the total myosin concentration. Scattering coefficients for monomers, tetramers, and minifilaments (octamers) were obtained from light scattering measurements where these were essentially the only species present. Scattering coefficients of other species were estimated from the measured values.

### Sedimentation Coefficient Modeling

Sedimentation coefficients for several different minifilament and assembly intermediate models were computed on a Macintosh-II computer by the

method of Garcia de la Torre and Bloomfield (1981) using the computer program GENTRA. This method involves modeling the molecular structure as a series of spheres. The program then uses an iterative approach to compute the translational frictional coefficient for the model which can be used to calculate the sedimentation coefficient. For the minifilaments and assembly intermediates discussed here, models typically contained 80–90 spheres. A hydration level of 0.3 gm water per gram of protein was used throughout.

## Results

### Myosin-II Minifilament Structure

Detailed electron microscopic studies indicate that *Acanthamoeba* myosin-II minifilaments are octamers. Negatively stained minifilaments (Fig. 1 *a*; Pollard, 1982) are highly homogeneous but the heads are generally poorly resolved. Two heads can occasionally be seen attached to a common stalk which extends slightly away from the minifilament backbone. Rotary-shadowed minifilaments are also homogeneous in size and routinely have clearly resolvable globular projec-

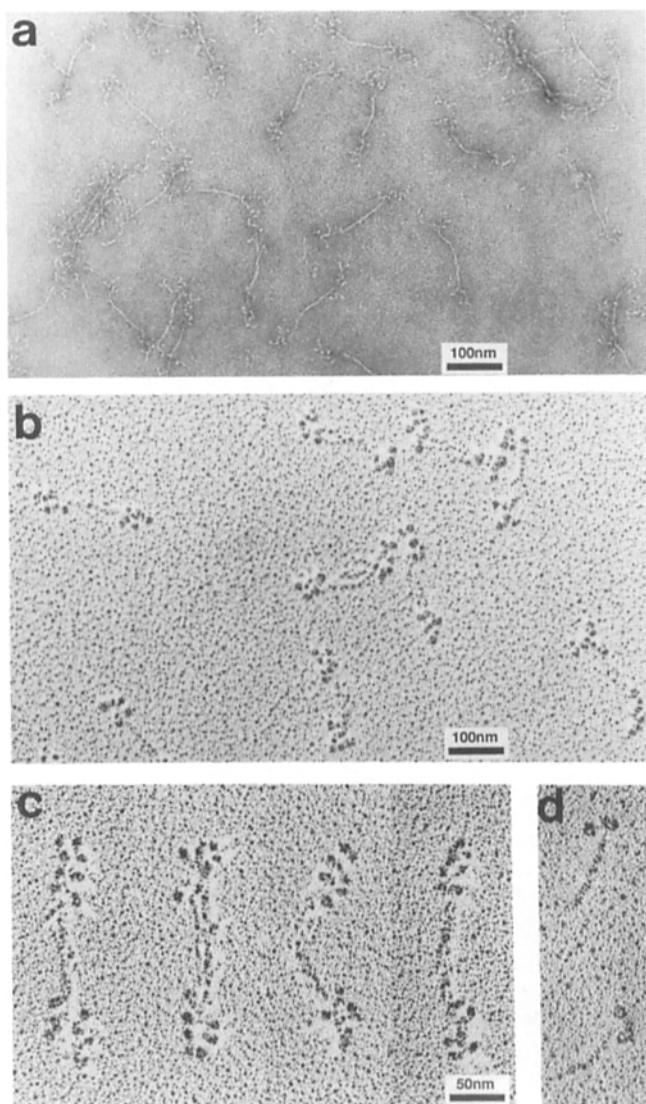


**Figure 1.** Myosin-II minifilaments. 10 mM imidazole, pH 7.0. (a) 10  $\mu\text{g}/\text{ml}$  myosin-II, 25 mM KCl. (b) 50  $\mu\text{g}/\text{ml}$  myosin-II, 25 mM KCl. (c) 20  $\mu\text{g}/\text{ml}$  myosin-II, 50 mM KCl. (d) 300 mM KCl.

tions (Fig. 1, *b* and *c*) the size of individual myosin heads (Fig. 1 *d*). These heads are closely apposed to the minifilament backbone, but the backbone itself is occasionally disrupted during the spraying and drying of the samples onto mica. In many of the rotary shadowed images (see especially Fig. 1 *c*) and in occasional negatively stained images, eight distinct heads can be counted in each half filament, indicating that the minifilament contains eight myosin molecules per minifilament.

The mean lengths ( $\pm$  SD) of the minifilaments are  $234 \pm 10$  nm for rotary shadowed images and  $229 \pm 8$  nm for negatively stained minifilaments, the difference probably due to the slightly looser association between the molecules in the negatively stained images. The bare zone length, measured as the distance between the points of attachment of the innermost pairs of heads of each half filament, is  $117 \pm 6$  nm for images visualized by both of the techniques. The axial stagger between heads is difficult to measure because of the variability in the way the heads align relative to the minifilament backbone, but in well-aligned examples it measures  $\sim 15$ – $16$  nm. A value of 15.5 nm, in good agreement with the measured value, can be calculated by subtracting the mean bare zone length from the mean minifilament length, subtracting the length of the heads at the two ends of the filament ( $\sim 11$  nm/head) and dividing the resulting value by six.

In both the negatively stained and rotary-shadowed preparations, occasional examples can be seen in which there are approximately twice as many heads per filament than in the usual case, although the dimensions of the filaments are not altered. These structures are believed to be two minifilaments laterally aggregated in register. The rotary shadowed samples of minifilaments also contain small, variable numbers of monomers and other partially assembled structures. These are believed to be filaments artifactually disassembled by shear forces during the drying process.

### Light Scattering of Myosin-II at Intermediate KCl and pH

Light scattering experiments under conditions between those promoting full assembly or complete disassembly indicate the presence of partially assembled minifilaments. The light scattering intensity of myosin-II in 50 mM KCl (minifilaments) or in 300 mM KCl (monomers) is proportional to the myosin-II concentration (Fig. 2 *a*) indicating that a single, homogeneous species is present in solution at each of these salt concentrations (see Sinard and Pollard, 1989, for details of the light scattering assay). For a fixed myosin concentration, increasing the KCl over the range of 100–200 mM causes a gradual decrease in the light scattering intensity (Sinard and Pollard, 1989; Fig. 1 *a*). With increasing KCl between 100 and 200 mM, the slope of a plot of light scattering vs. myosin concentration decreases and becomes non-linear (Fig. 2 *a*). Although smooth curves fit these data well, we have drawn lines with breaks, indicated by arrows, to emphasize that the point of maximum curvature in each of these plots occurs between 40 and 50  $\mu\text{g}/\text{ml}$  (100–125 nM).

At low concentrations of KCl, alkaline pH reduces the slope of plots of light scattering vs. myosin concentration (Fig. 2 *b*). Unlike the plots at various KCl concentrations, the data for each pH can be fit by a single straight line passing essentially through the origin. Variation of the pH has no effect on the light scattering of myosin-II in high salt (Fig. 2 *b*).

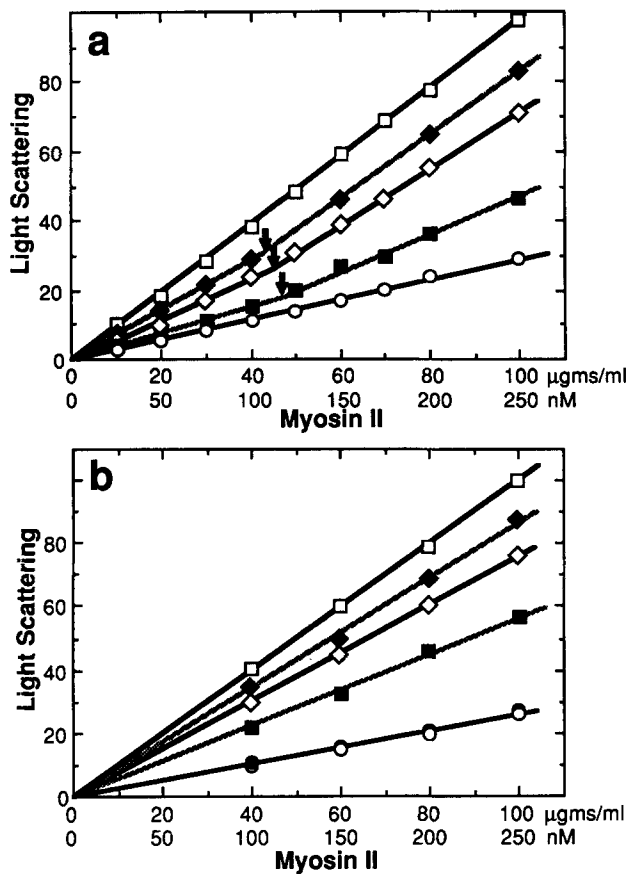


**Figure 2.** Light scattering intensity (at 365 nm) of myosin-II as a function of salt, pH, and myosin concentration. Light scattering is expressed in arbitrary units. (a) 1.3% sucrose, 8.5 mM imidazole, pH 7.0, 1.2 phosphates per myosin molecule, myosin concentration as indicated, KCl (□) 50 mM, (◆) 135 mM, (◇) 150 mM, (■) 175 mM, (○) 300 mM. Arrows indicate points at which the fit lines are discontinuous. (b) 1.0% sucrose, 9 mM imidazole or bicine, 1.1 phosphates per myosin molecule, myosin concentration as indicated: 50 mM KCl, pH (□) 7.0, (◆) 7.8, (◇) 8.6, (■) 9.2; 300 mM KCl, pH (●) 7.0, (○) 9.2.

### Analytical Ultracentrifugation of Myosin-II Assembly Intermediates

Under conditions where myosin-II is monomeric (300 mM KCl; see Sinard and Pollard, 1989) or fully assembled into minifilaments (50 mM KCl), the myosin sediments as a single, major symmetrical peak. The sedimentation coefficients are 7–8 S for monomers and ~21.5 S for the minifilaments (Fig. 3). These sedimentation coefficients are independent of protein concentration in the range of 100–500  $\mu\text{g/ml}$  (~0.2–1.0  $\mu\text{M}$ ) (data not shown). In 50 mM KCl, a variable but small amount of material also sediments at ~8 S, probably representing monomer which is either in equilibrium with the polymer or incompetent to assemble.

At neutral pH and KCl concentrations between 100 and 200 mM, myosin-II sediments as at least three discrete species in salt and myosin concentration dependent equilibrium with each other (Fig. 4 a). In 100 mM KCl, the major peak is at ~19 S (Fig. 4 a) and is broader than the 21.5 S peak at 50 mM KCl (Fig. 3). This reaction boundary presumably represents minifilaments whose sedimentation rate is shifted

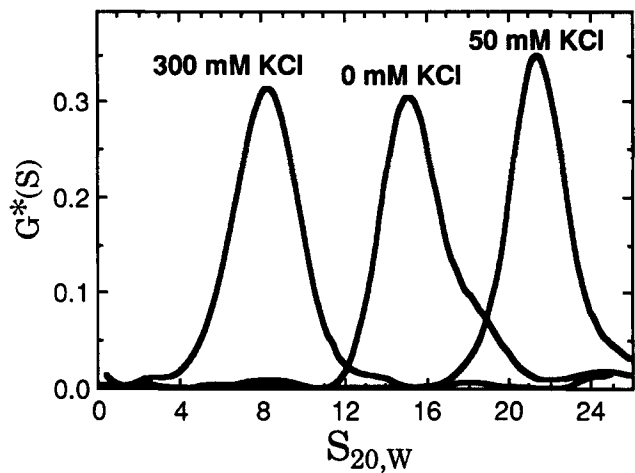


**Figure 3.** Velocity sedimentation of myosin-II. Myosin-II at 500  $\mu\text{g/ml}$  was sedimented at 20°C in 9 mM imidazole, pH 7.0, 5% sucrose, and either 0, 50, or 300 mM KCl, at a rotor speed of 34,000 rpm. Sedimentation coefficients have been corrected to water.  $G^*(S)$ , which represents the relative amount of species with a given sedimentation coefficient, is expressed in arbitrary units.

to a lower apparent sedimentation coefficient by rapid equilibration with a small amount of lower molecular weight species. In support of this, a small amount of material is present at the monomer position. At 125 mM KCl, the reaction boundary is smaller, shifts to a lower sedimentation coefficient, and acquires a shoulder in the region of 13 S (Fig. 4 a). More material is seen in the monomer position. With increasing salt, the major mass of sedimenting material shifts from the 21.5 S “minifilament” peak, through an intermediate species at ~13 S, to the slower sedimenting “monomer” peak near 7 S. The species at ~13 S is always present as a distinct peak or as a shoulder on another peak, and can also be seen in sedimentation runs at 120, 140, and 160 mM KCl (data not shown).

Sedimentation of myosin at 0.16–1.57 mg/ml (~0.4 to 3.7  $\mu\text{M}$ ) shows a concentration dependent shift of material into peaks with higher sedimentation coefficients (Fig. 4 b). This is indicative of a system in concentration-dependent assembly equilibrium. The small shoulder seen at approximately 9.5 S in all of these curves and the increasing height of the curves between the 7 S and the 13 S position with increasing concentration (Fig. 4 b) indicate that another species exists in this region, with a sedimentation coefficient of ~9–10 S. These curves show no evidence for a species sedimenting between 13 S and 21.5 S.

Light scattering studies (Sinard and Pollard, 1989) have shown a drop in light scattering intensity of myosin-II minifilaments at very low salt concentrations, suggesting that partial minifilament disassembly is occurring. In 10 mM imidazole, 0 mM KCl, myosin-II sediments as a single major 15 S peak with a shoulder suggesting that this species is in equilibrium with a higher molecular weight species (Fig. 3). This confirms that the peak/shoulder seen in the region of 15 S for sedimentation experiments at salt concentrations between 100 and 200 mM KCl (Fig. 4) is a real species and not simply a reaction boundary.

A two-species plot from the ultracentrifugation of myosin-II to equilibrium in the absence of KCl (Fig. 5 a) is linear,

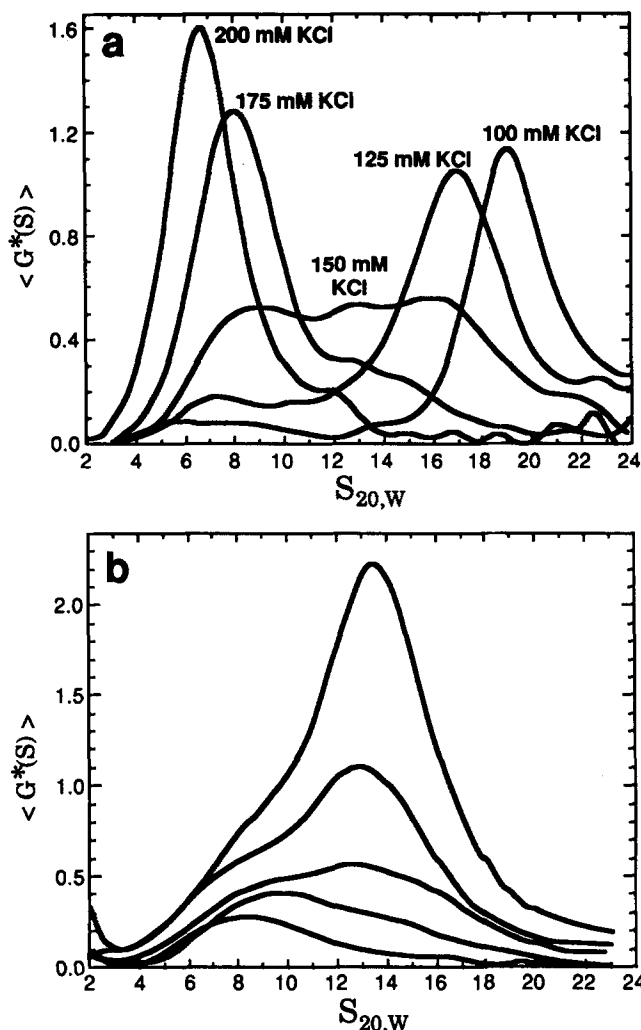


**Figure 4.** Velocity sedimentation of myosin-II assembly intermediates. Myosin-II was sedimented at 20°C in 9 mM imidazole, pH 7.0, 5% sucrose at a rotor speed of 34,000 rpm.  $G^*(S)$  represent the average of six time points and is expressed in arbitrary units. (a) Salt dependence of sedimentation profiles: 0.52 mg/ml myosin-II; 200, 175, 150, 125, or 100 mM KCl, as indicated. (b) Concentration dependence of sedimentation profiles at 150 mM KCl: myosin-II concentrations of (lowest to highest curves) 0.16, 0.29, 0.52, 0.89, 1.57 mg/ml.

indicating that only two major assemblies of myosin-II are formed as a function of concentration in 0 mM KCl. Extrapolation of a line passing through these points to the hyperbola shown gives the molecular weights of the smallest and largest species present in significant amounts under these conditions. These molecular masses are 1,700 and 3,600 kD, respectively. Assuming a monomer hydrodynamic molecular mass for myosin of ~430 kD (Stafford, W. F., and T. D. Pollard, unpublished data), this corresponds to oligomers consisting of 4.0 and 8.4 myosin molecules each, or a tetramer–octamer equilibrium. The data is inconsistent with the existence of a significant amount of any species intermediate in size between the tetramer and the octamer.

Equilibrium ultracentrifugation of myosin in 200 mM KCl and in 50 mM KCl provides further evidence for the existence of discrete assembly intermediates (Fig. 5, b and c).

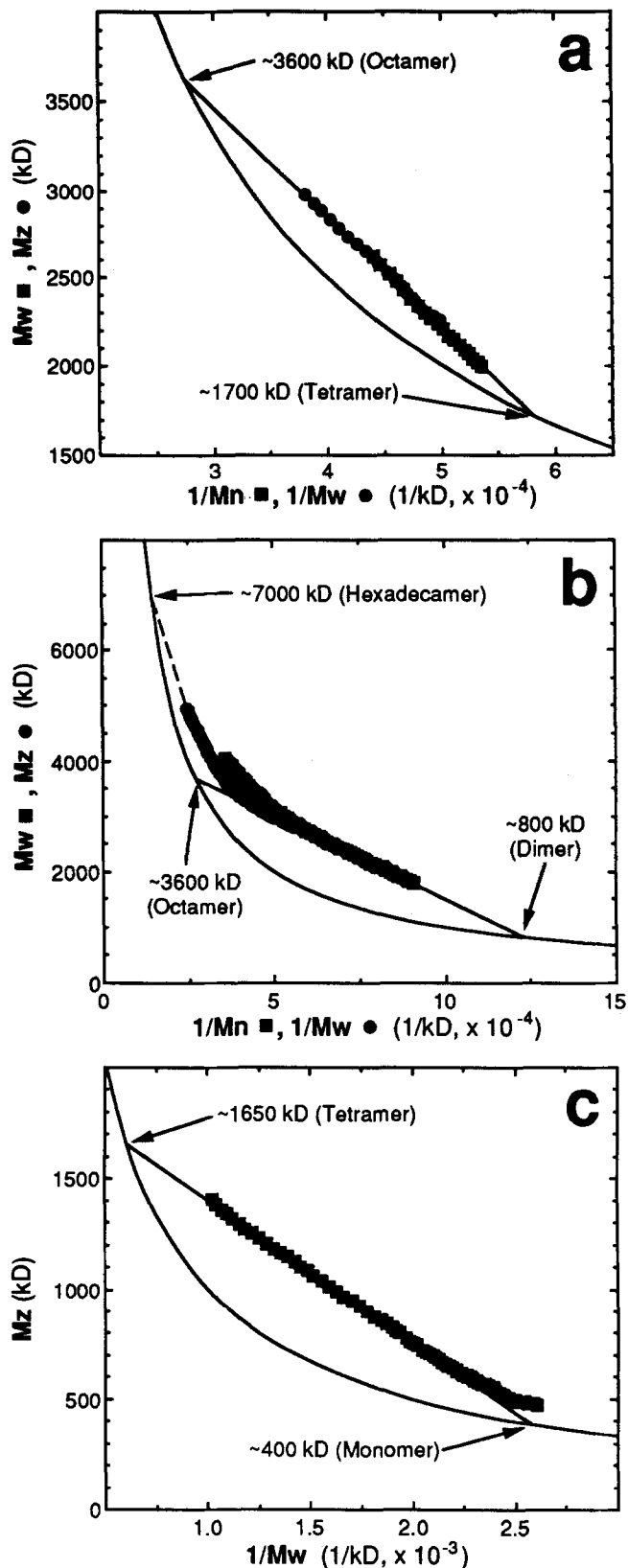


**Figure 5.** Two species plots from centrifugation to equilibrium of myosin-II. Myosin-II at 500  $\mu$ g/ml in 9 mM imidazole, pH 7.0, .02% azide, and KCl concentrations as indicated below was centrifuged to equilibrium at 4°C. Salt concentrations, rotor speeds, and time of centrifugation were (a) 0 mM, 6 krpm, 5 d; (b) 50 mM, 4 krpm, 6 d; (c) 200 mM, 8 krpm, 5 d.

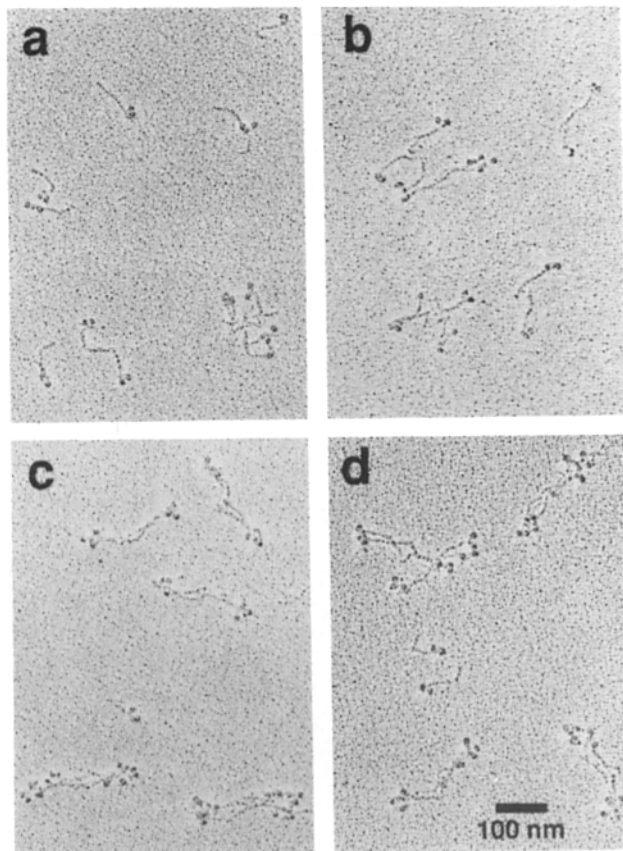


**Figure 6.** Effect of salt on myosin-II minifilament assembly. Electron micrographs of rotary shadowed myosin-II (40  $\mu\text{g}/\text{ml}$ ) in 5 mM imidazole, pH 7.0, and KCl concentration of (a) 175, (b) 150, (c) 100, and (d) 75 mM. (e) Distribution of myosin molecules among assembly forms as a function of salt concentration in randomly selected electron microscopic fields. Because it was not always possible to resolve all of the heads, structures in which six or more molecules were clearly visible were counted as minifilaments (octamers).

A two-species plot of the 200 mM KCl run indicates a monomer-tetramer equilibrium. The run at 50 mM KCl is somewhat more complex and suggests a dimer-octamer equilibrium over most of the protein concentration range. However, at protein concentrations  $>\sim 0.5$  mg/ml (leftmost data points), there is a significant amount of hexadecamer.

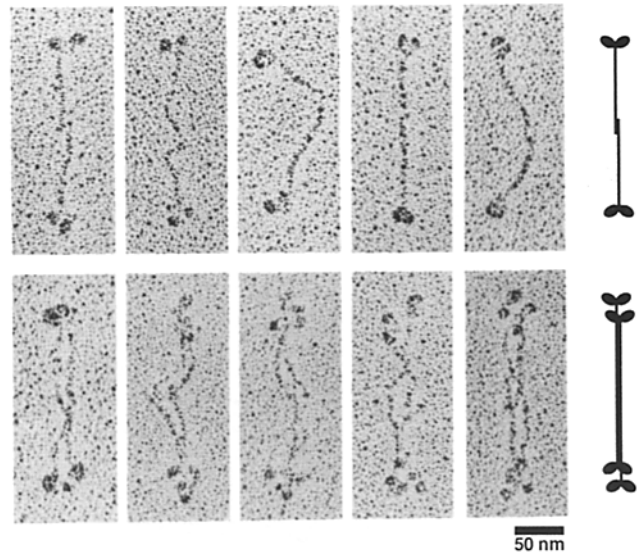


**Figure 7.** Myosin-II minifilament assembly intermediates. *Top row*, antiparallel dimers. *Bottom row*, antiparallel tetramers.

### Electron Microscopic Visualization of Intermediates in the Assembly of Myosin-II Minifilaments

Electron microscopy of myosin-II sprayed onto mica and rotary shadowed revealed directly the structures of the assembly intermediates detected by analytical ultracentrifugation (Figs. 6 and 7). Although shear forces and the transient increase in the concentration of the nonvolatile KCl during the drying process both contribute to making a sample at a given salt concentration appear less assembled when visualized by this technique, cross-linking reagents were not used since they were found to artifactually shift the rapid equilibrium between intermediates far in favor of the fully assembled state (data not shown).

The first assembly intermediate seen is the antiparallel dimer. Above  $\sim 200$  mM KCl, monomers comprise  $>95\%$  of the structures visualized, but in 150–175 mM KCl (Fig. 6, a and b and Fig. 7, *top row*), 15–20% of the myosin-II molecules form antiparallel dimers (Fig. 6 e) with a mean head to head distance of  $161 \pm 7$  nm. Since the monomer tails are 87 nm long, the overlap in the antiparallel dimer is 13–15 nm. In some examples, the dimer is only partly associated (see Fig. 11). Measurements of these images confirm a 15-nm overlap and suggest that the antiparallel dimer is formed by interaction between the very end of a myosin-II tail and a point  $\sim 15$  nm from the tip of the tail of a second myosin-II molecule. No parallel dimers were observed.

At KCl concentrations of 100–125 mM, tetramers  $203 \pm 8$  nm long are the predominant species (Fig. 6 c and Fig. 7, *bottom row*). Occasional examples can be seen in which two antiparallel dimers seem to associate to form the tetramer (see Fig. 11). We never observed trimers or monomers adding onto dimers. This suggests that the antiparallel tetramer is formed by the lateral association of two antiparallel dimers, and the size of the tetramer, taking into account the dimensions of the heads and the dimer head-to-head distance, indicates that the axial stagger of the two antiparallel dimers is  $\sim 15$  nm.

Below  $\sim 75$  mM KCl, full size octameric minifilaments are the predominant species observed (Fig. 6 *d*). Their dimensions are consistent with being formed by the lateral association of two antiparallel tetramers axially staggered by 30 nm. Electron microscopic images can be seen in which two tetramers are positioned next to each other with this stagger, suggesting that they may be associating (or dissociating) to form a minifilament. We never observed an antiparallel dimer associating with a tetramer to form a hexamer.

In 0 mM KCl, images are essentially the same as seen at 50 mM KCl in which fully formed minifilaments predominate (data not shown).

The assembly state of myosin-II can also be altered by varying the pH (Pollard, 1982; Sinard and Pollard, 1989). At low pH, minifilaments aggregate to form thick filaments (Fig. 8 *a*). Above neutral pH, however, the filaments depolymerize, and the assembly intermediates formed (Fig. 8, *b-f*) are essentially the same as were seen for KCl induced minifilament disassembly. A potentially new intermediate was occasionally seen when pH was used to disassemble minifilaments. These appeared to contain six myosin heads on each half filament. The field in Fig. 8 *c* was selected to emphasize these potential hexamers, which were actually few in number.

## Discussion

### Myosin-II Minifilaments Are Octamers

Previous studies on the structure of the myosin-II minifilaments (formerly termed "thin filaments"; Pollard et al., 1978; Pollard, 1982) indicated that the filaments were  $\sim 205$  nm long with the four rows of heads in each half filament separated by 15 nm. Since occasional examples were found with two pairs of heads in one row, it was postulated (Pollard, 1982) that each minifilament contained at most 16 myosin-II molecules.

The current study suggests that, although this structure of the filament is essentially correct with four rows of heads in each half filament staggered by 15 nm, only one pair of heads is in each row of heads in the minifilament, and the octamer is in fact the most prevalent species in 20–100 mM KCl. There are multiple lines of evidence for this. The first, and perhaps most direct, is the electron microscopic images of rotary shadowed myosin-II minifilaments, which, in many cases, clearly show eight myosin heads per half filament and thus eight myosin-II molecules per minifilament.

Secondly, velocity sedimentation experiments show that the myosin-II minifilaments have a sedimentation coefficient of  $\sim 22$  S, in good agreement with literature values (Kuznicki et al., 1983), and computer modeling suggests that this structure cannot be a hexadecamer. Using the minifilament dimensions obtained from this study (total length = 232 nm; bare zone length = 117 nm; 15-nm spacing between rows of heads), we constructed models composed of 94 and 76 spheres to model the mass distribution expected for an octameric and hexadameric minifilament, respectively. We then used the method of Garcia de la Torre and Bloomfield (1981) to calculate theoretical frictional coefficients and thus sedimentation coefficients for the two models. This yielded a value of 22.7 S for the octamer, in good agreement with the measured 22 S value. The calculated value for the hexadecamer, 40.5 S, is

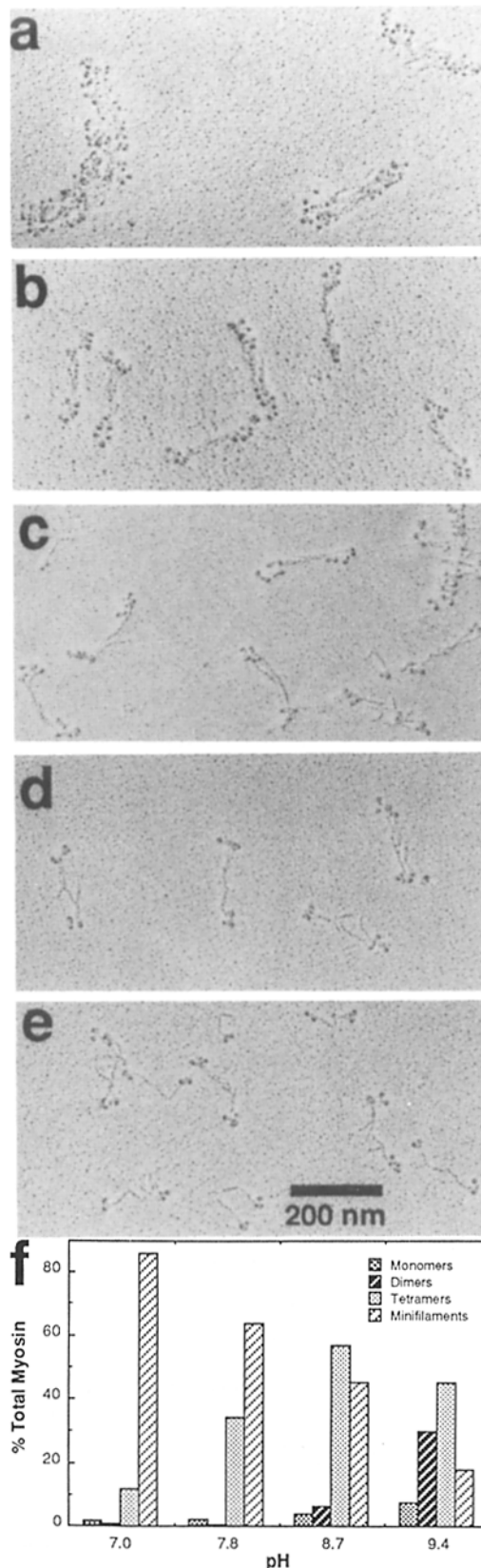


**Figure 8.** Effect of pH on myosin-II minifilament assembly. Electron micrographs of rotary shadowed myosin-II (40  $\mu$ g/ml) in 50 mM KCl, and 5 mM imidazole or bicine, pH (a) 6.2, (b) 7.0, (c) 7.8, (d) 8.7, and (e) 9.4. (f) Distribution of myosin among assembly forms as a function of pH, determined as described in legend for Fig. 6.

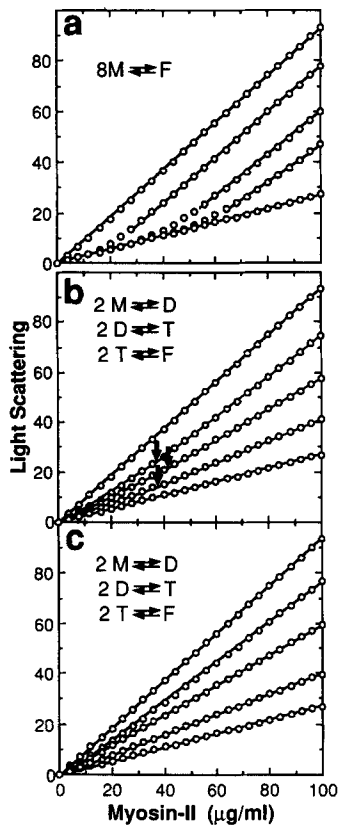


**Figure 9.** Theoretical plots of light scattering vs. myosin-II concentration. Circles represent the theoretical light scattering intensity as calculated from a computer simulated equilibrium based on the models shown. Lines represent linear fits to the theoretical data. Arrows indicate points at which the slope of the line changes to a new value. (a) Monomer-octamer equilibrium. Equilibrium association constants for the five simulations are  $10^{-5}$ ,  $10^{-13}$ ,  $2 \times 10^{-16}$ ,  $10^{-17}$ , and  $10^{-20} \text{ M}^{-7}$ . (b and c) Monomer-dimer-tetramer-octamer equilibrium. Equilibrium association constants for the three equilibria for each of the five simulations in  $\text{M}^{-1}$  are (b) 1, 10, 10; 0.1, 0.5, 0.02; 0.1, 0.1,  $10^{-3}$ ; 0.1,  $10^{-3}$ ,  $10^{-6}$ ;  $10^{-5}$ ,  $10^{-8}$ ,  $10^{-8}$ . (c) 1, 10, 10; 1, 10, 0.015; 1, 1,  $10^{-8}$ ; 1,  $10^{-4}$ ,  $10^{-10}$ ;  $10^{-5}$ ,  $10^{-5}$ ,  $10^{-10}$ .

much larger. In support of this interpretation, skeletal muscle myosin in 5 mM citrate/Tris buffer, pH 8.0, forms a 22 S species, which was identified by viscosity, diffusion, and multiple angle light scattering experiments to be an octamer (Reisler et al., 1986).

Finally, equilibrium ultracentrifugation in 50 mM KCl has shown the predominant equilibrium to be between a dimer and an octamer. Only at very high protein concentrations ( $>0.5 \text{ mg/ml}$ ), significantly above the cellular concentration of myosin-II ( $\sim 0.25 \text{ mg/ml}$ ; Kiehart and Pollard, 1984), does one see significant dimerization of the octameric minifilament to form a hexadecamer.

#### Light Scattering Studies and Computer Modeling Indicate the Presence of Assembly Intermediates

The salt dependence of myosin-II assembly (Sinard and Pollard, 1989) indicates that minifilaments predominate between 20 and 100 mM KCl, and that myosin is monomeric above 200 mM KCl. Between 100 and 200 mM KCl, there is a gradual decrease in the light scattering intensity of a fixed concentration of myosin. To investigate whether this decrease was due to a shift in the equilibrium between fully formed minifilaments and monomers or to the presence of partially assembled minifilaments, we determined the dependence of light scattering intensity on the myosin concentration at KCl concentrations in this range. The slope of these plots at a given myosin concentration indicates the size of the structures being formed as the myosin concentration is increased from that concentration. At any salt concentration, if all of the myosin exists in one form independent of protein concentration, the plot will be linear, pass through the ori-

gin, and have a slope dependent on the size of the polymer. This is what is seen for myosin in high salt (monomers) and low salt (minifilaments). At all intermediate KCl concentrations, the situation is more complex: the light scattering intensity is directly proportional to the myosin concentration up to  $\sim 40\text{--}50 \text{ }\mu\text{g/ml}$ , but at higher concentrations, the slope is larger. On both sides of the "break", the slope decreases with increasing KCl concentration. Increasing the pH at 50 mM KCl has a similar effect on these plots, but no break is seen; the data can be fit by a single straight line.

Computer modeling of equilibria to predict plots of light scattering intensity vs. myosin-II concentration for various models (Fig. 9) showed that a monomer-dimer-tetramer-octamer equilibrium is consistent with the data, and that simpler models are not. For example, a simple equilibrium between monomer and octamer, in which the equilibrium constant varies with the ionic strength of the solution, predicts a critical concentration phenomenon for any equilibrium constant (Fig. 9 a). Below this concentration, all of the myosin-II is monomeric. Above the critical concentration, all additional myosin is assembled into minifilaments. The exponent of eight in the equilibrium reaction is responsible for the rather abrupt break in the plot. Changing the equilibrium constant changes the critical concentration, and thus the point at which this transition occurs, but has no effect upon the slope of the curve before or after the break. This was shown to be the case for skeletal muscle myosin synthetic filament assembly (Josephs and Harrington, 1966). Such a model cannot simulate data with varying slopes as observed for *Acanthamoeba* myosin-II. Similarly, a model with monomer in equilibrium with dimer and dimer in equilibrium with octamers is inadequate. Although this model begins to fit the observed dependence of myosin-II light scattering on the KCl concentration, it did not come close to fitting the pH dependence (data not shown).

The only models that could adequately account for both the observed KCl dependence and the observed pH dependence included a higher order intermediate, either a tetramer or a hexamer. Sample theoretical light scattering curves for the model monomer-antiparallel dimer-antiparallel tetramer-octamer are shown in Fig. 9, b and c. Note that in Fig. 9 b, the curve breaks seen for the KCl dependence curves (Fig. 2 a) at  $\sim 50 \text{ }\mu\text{g/ml}$  total myosin concentration could be modeled. A different rate of variation of the three equilibrium constants in this model produced the theoretical curves shown in Fig. 9 c which closely approximate the observed pH dependence plots (Fig. 2 b). Other models with more intermediates could also fit the data, and so the concordance of the model and the data does not prove that the model is correct. This approach, however, is useful in that it can rule out models which cannot fit the data, and in that it has shown that assembly intermediates must be present at salt concentrations in the range of 100–200 mM KCl.

#### The Assembly Intermediates Are Tetramers and Antiparallel Dimers

The predominant minifilament assembly intermediate detected by analytical ultracentrifugation and electron microscopy is the antiparallel tetramer. Velocity sedimentation studies indicate the presence of a 13–14-S intermediate between monomer or monomer/dimer and full length minifilament (octamer) at KCl concentrations between 100 and 200

mM, and show that this structure is in equilibrium with both more rapidly and more slowly sedimenting species. At very low ionic strength, this intermediate is the major species present, and equilibrium ultracentrifugation has identified it as a tetramer in equilibrium with octamer. Electron microscopy of myosin-II in 100–150 mM KCl reveals an antiparallel tetramer, and computer modeling of this species predicts a sedimentation coefficient of 13.8 S. (Electron microscopy of zero salt specimens revealed only octamers, which we attribute to the transient increase in the salt concentration during drying.)

Antiparallel dimers are a second assembly intermediate. The concentration dependence of the velocity sedimentation profiles at 150 mM KCl (Fig. 4 b) suggested the presence of an  $\sim 9$ -S species. Equilibrium ultracentrifugation of myosin-II in 50 mM KCl (Fig. 5 b) identified a dimer in equilibrium with minifilaments, and electron microscopy revealed an antiparallel dimer with a 15-nm overlap of the tails. Computer modeling of the sedimentation coefficient for this antiparallel dimer predicts a value of 8.3 S, in good agreement with the measured value.

The antiparallel dimers and tetramers are likely to be true assembly intermediates, rather than side reaction products. The structures of these intermediates are subsets of the complete minifilament. Therefore, disassembly of the intermediates or some other gross structural change is not necessary for incorporation into a completed minifilament. Velocity sedimentation and equilibrium ultracentrifugation experiments suggest that these intermediates are in a concentration dependent, reversible equilibrium with each other and with monomer and minifilament. Finally, the distribution of myosin among monomers, dimers, tetramers, and octamers as a function of the KCl concentration (Fig. 6 e) is precisely as one would predict for a mechanism in which the dimer and tetramer are assembly intermediates between monomers and octamers.

### *Minifilaments Assemble by Three Sequential Dimerization Steps*

Data from light scattering, analytical ultracentrifugation, and electron microscopy allow us to propose a model for the assembly mechanism of *Acanthamoeba* myosin-II minifilaments, shown diagrammatically in Fig. 10 and with electron micrographs in Fig. 11. Assembly occurs in three steps, and each step is a dimerization. Initially, monomers assemble to form an antiparallel dimer with a 15-nm overlap at the ends of each of the tails. Then, two antiparallel dimers associate with a 15-nm axial stagger to form an antiparallel tetramer. Finally, two tetramers dimerize, with an axial stagger of 30 nm, to form the completed, octameric minifilament.

Multiple lines of evidence suggest that the transition from tetramer to octamer is direct and does not proceed via a hexamer. First, electron microscopy failed to show any associations between dimers and tetramers to form hexamers, whereas every grid examined contained examples of two tetramers associating to form an octamer. Second, Fig. 6 e shows that at 100 mM KCl, where  $\sim 45\%$  of the myosin is in the form of tetramers, only  $\sim 25\%$  of the myosin still exists as monomers or dimers. This means that if a hexamer were an obligate intermediate in the pathway to octamers, some of the already formed tetramers would have to depolymerize to at least dimers to increase the dimer pool and allow the re-

maining tetramers to form hexamers and then octamers. Although this is possible, preliminary kinetic experiments indicate that minifilament assembly is extremely rapid, occurring within milliseconds. A rapid off-rate would be required to complete the assembly in a short period of time, and the very low critical concentration ( $<5$  nM; Sinard and Pollard, 1989) suggests that the off rate is not very fast. Third, velocity sedimentation experiments have failed to indicate the presence of a discrete species sedimenting between the 13 S tetramers and the 21.5 S octamers. Computer modeling of the theoretical hexameric intermediate yields a sedimentation coefficient of 18.8 S, which should show up as a significant shoulder on sedimentation coefficient plots made at the lower salt concentrations in Fig. 4 a. Finally, the equilibrium ultracentrifugation experiment in 0 mM KCl showed only two species, tetramer and octamer, and gave no evidence of the existence of a hexamer, which would have been detected by this technique.

Equilibrium ultracentrifugation experiments in 50 mM KCl indicate that at very high myosin-II concentrations ( $>0.5$  mg/ml), there is some dimerization of octameric minifilaments to form hexadecamers. Although the measured sedimentation coefficient of 21.5 S for the minifilament indicates that hexadecamers can constitute only a very minor species at physiological myosin-II concentrations, they may explain the earlier identification of 16 as the upper limit for the number of molecules per minifilament (Pollard, 1982).

One apparently inconsistent piece of data is the equilibrium centrifugation experiment done at 200 mM KCl, which showed a monomer-tetramer equilibrium with no evidence of a dimer intermediate. This is perhaps explained by the fact that the electron microscopy data indicate that even at concentrations as low as 40  $\mu$ g/ml, dimers never constitute  $>20\%$  of the total mass of the myosin. If the association of two dimers to form tetramers is a very concentration sensitive step, it is not unlikely that the dimers would constitute only a very small percentage of the myosin present at the higher protein concentrations needed for the equilibrium ultracentrifugation experiment and therefore would not be detected by this method.

Unlike salt-induced disassembly, pH-induced disassembly occasionally produced intermediates that appeared to be hexamers. Although these structures may represent "artifacts" of the electron microscopy, since solvent conditions do alter the extent to which the heads associate with each other and therefore may be poorly resolved, we cannot rule out a possible alternative assembly pathway involving a hexamer when pH is used to modulate the assembly state. Further equilibrium and kinetic experiments will be necessary to resolve this question.

Atkinson and Korn (1987) proposed an alternative model for myosin-II minifilament assembly that is based on parallel dimers. In their model, the initial species formed is a parallel dimer with subunits staggered axially by 30 nm. Two of these dimers form an antiparallel tetramer, different from the tetramer described above in that the heads are staggered by 30 nm. These tetramers assemble with a 15-nm stagger to form a minifilament. Their model was based on electric birefringence studies of myosin-II from which the COOH-terminal 66 amino acids had been removed by chymotryptic cleavage (Wijmenga et al., 1987). This modified myosin-II forms a 30-nm staggered dimer under polymerizing condi-

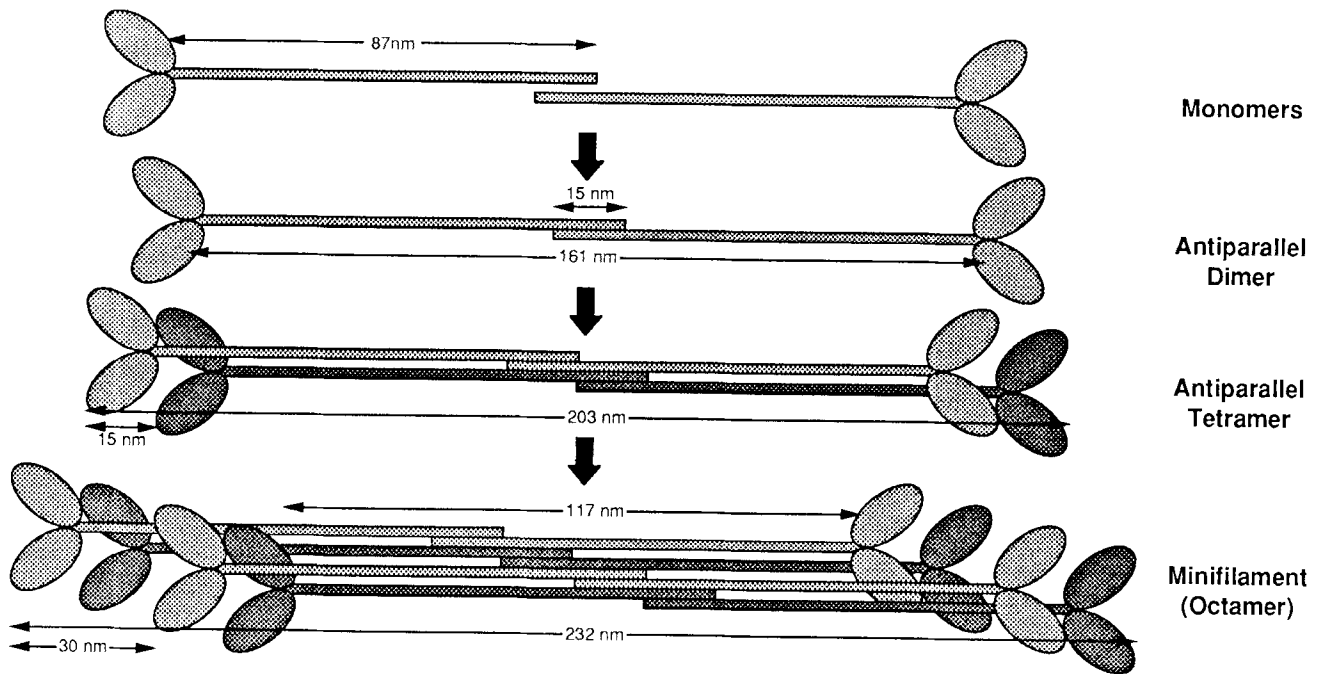


Figure 10. Diagrammatic model for the assembly mechanism of myosin-II minifilaments.

tions (Kuznicki et al., 1985). We looked by electron microscopy for the intermediates postulated in the Atkinson and Korn model but observed none of them. However, we can reconcile their data with ours by suggesting that the dimerization of chymotryptically cleaved myosin actually corresponds to the last step in the assembly process rather than the first. This explanation is plausible because the terminal  $\sim 10$  nm of the tail are required to form antiparallel dimers and tetramers.

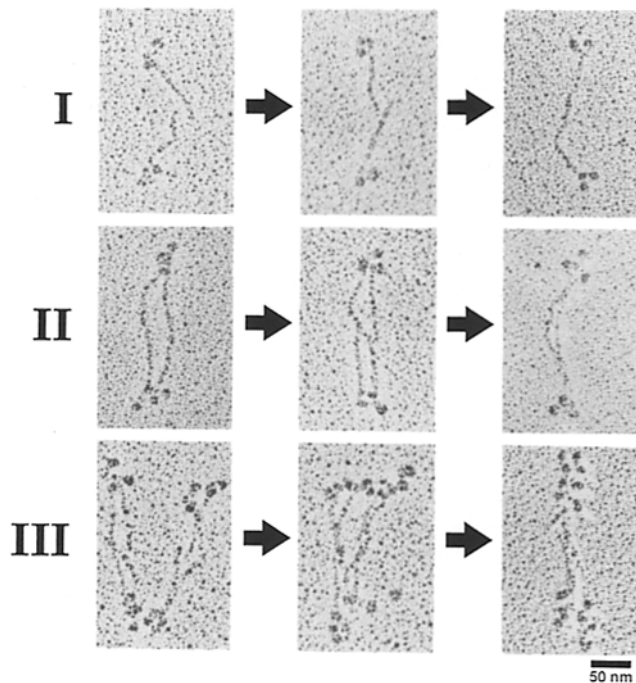


Figure 11. Model for the assembly mechanism of myosin-II minifilaments using electron microscopic images.

#### The *Acanthamoeba* Myosin-II Assembly Mechanism May be Shared by Other Myosins

Although no other system has yet been analyzed in detail, the mechanism of assembly of *Acanthamoeba* myosin-II minifilaments described here (Figs. 10 and 11) may apply to myosin-II from other sources. Under very low ionic strength conditions, *Dictyostelium* myosin-II forms antiparallel dimers and tetramers, although the subunit stagger in the tetramers was not reported (Kuczmarski et al., 1987). However, parallel dimers are also seen. Skeletal muscle myosin minifilaments are hexadecameric (Reisler et al., 1980). In the absence of KCl, decreasing the buffer concentration leads to conversion of the minifilaments to octamers, and at still lower concentrations to tetramer formation (Reisler et al., 1986).

We have shown here that the initial step in *Acanthamoeba* myosin-II minifilament assembly is the formation of an antiparallel dimer. Detailed kinetic analyses of the assembly of pH 8.0 synthetic filaments from skeletal muscle myosin have revealed that a parallel dimer is involved in the elongation phase of assembly (Davis, 1981a,b, 1985; Davis et al., 1982) but this work does not directly address the formation of the bare zone. Unreported experiments as well as experiments by other groups (reviewed in Davis, 1988) have indicated that the nucleation rate depends on the square of the myosin concentration, and although some data suggests that a parallel dimer may also be involved in this step, an antiparallel dimer, as has been shown here to be the key species for *Acanthamoeba* myosin-II, cannot be ruled out.

Bare zone nucleation in other myosin systems may proceed in a fashion similar to the minifilament assembly mechanism characterized here. Nonetheless, it appears that the ability to form parallel dimers is necessary to form structures much longer than minifilaments. This is seen with both skeletal muscle myosin and *Dictyostelium* myosin-II, but *Acanthamoeba* myosin-II, which does not form parallel dimers

under normal conditions, does not elongate. This suggests that the same region or regions of the myosin tail which promote parallel dimer formation are also likely to be involved in the interactions which occur during the elongation process. Since both skeletal muscle myosin and *Dictyostelium* myosin-II have much longer tails than *Acanthamoeba* myosin-II, it is reasonable to assume that such a region might be absent from the *Acanthamoeba* myosin-II tail.

We would like to thank Pam Maupin for her assistance in preparing the samples for electron microscopy, and Dr. Julien Davis for his critical reading of the manuscript.

This work was funded by a Medical Scientist Training Program award to J. H. Sinard (GM-07309), and National Institutes of Health research grants to T. D. Pollard (GM-26132) and to the Boston Biomedical Research Institute (W. F. Stafford) (RR-05711).

Received for publication 10 April 1989 and in revised form 6 July 1989.

## References

- Ansevin, A. T., D. E. Roark, and D. A. Yphantis. 1970. Improved ultracentrifuge cells for high-speed sedimentation equilibrium studies with interference optics. *Anal. Biochem.* 34:237-261.
- Atkinson, M. A. L., and E. D. Korn. 1987. Appendix: a model for the polymerization of *Acanthamoeba* myosin-II and the regulation of its actin-activated Mg-ATPase activity. *J. Biol. Chem.* 262:15809-15811.
- Bridgman, W. D. 1942. Some physical chemical characteristics of glycogen. *J. Am. Chem. Soc.* 64:2349-2356.
- Clarke, M., and J. A. Spudich. 1974. Biochemical and structural studies of actomyosin-like proteins from non-muscle cells: isolation and characterization of myosin from amoeba of *Dictyostelium discoideum*. *J. Mol. Biol.* 86:209-222.
- Davis, J. S. 1981a. The influence of pressure on the self-assembly of the thick filament from the myosin of vertebrate skeletal muscle. *Biochem. J.* 197:301-308.
- Davis, J. S. 1981b. Pressure-jump studies on the length-regulation kinetics of the self-assembly of myosin from vertebrate skeletal muscle into thick filament. *Biochem. J.* 197:309-314.
- Davis, J. S. 1985. Kinetics and thermodynamics of the assembly of the parallel and antiparallel packed section of synthetic thick filaments of skeletal myosin: a pressure-jump study. *Biochemistry.* 24:5263-5269.
- Davis, J. S. 1988. Assembly processes in vertebrate skeletal thick filament formation. *Annu. Rev. Biophys. Biophys. Chem.* 17:217-239.
- Davis, J. S., J. Buck, and E. P. Green. 1982. The myosin dimer: an intermediate in the self-assembly of the thick filament of vertebrate skeletal muscle *FEBS (Fed. Eur. Biochem. Soc.) Lett.* 140:293-297.
- DeRosier, D. J., P. Munk, and D. J. Cox. 1972. Automatic measurement of interference photographs from the ultracentrifuge. *Anal. Biochem.* 50:139-153.
- Garcia de la Torre, J., and V. A. Bloomfield. 1981. Hydrodynamic properties of complex, rigid, biological macromolecules: theory and applications. *Q. Rev. Biophys.* 14:81-139.
- Hildebrand, F. B. 1956. Introduction to Numerical Analysis. McGraw-Hill, Inc., New York. 551 pp.
- Josephs, R., and W. F. Harrington. 1966. Studies on the formation and physical chemical properties of synthetic myosin filaments. *Biochemistry.* 5:3474-3487.
- Kiehart, D. P., and T. D. Pollard. 1984. Inhibition of *Acanthamoeba* actomyosin-II ATPase activity and mechanochemical function by specific monoclonal antibodies. *J. Cell Biol.* 99:1024-1033.
- Korn, E. D., and J. A. Hammer. 1988. Myosins of nonmuscle cells. *Annu. Rev. Biophys. Biophys. Chem.* 17:23-45.
- Kuczmarski, E. R., and J. A. Spudich. 1980. Regulation of myosin self-assembly: phosphorylation of *Dictyostelium* heavy chains inhibits formation of thick filaments. *Proc. Natl. Acad. Sci. USA.* 77:7292-7296.
- Kuczmarski, E. R., S. R. Tafuri, and L. M. Parysek. 1987. Effect of heavy chain phosphorylation on the polymerization and structure of *Dictyostelium* myosin filaments. *J. Cell Biol.* 105:2989-2997.
- Kuczmarski, E. R., L. Routsolias, and L. M. Parysek. 1988. Proteolytic fragmentation of *Dictyostelium* myosin and localization of the *in vivo* heavy chain phosphorylation site. *Cell Motil. Cytoskel.* 10:471-481.
- Kuznicki, J., J. P. Albanesi, G. P. Cote, and E. D. Korn. 1983. Supramolecular regulation of the actin-activated ATPase activity of filaments of *Acanthamoeba* myosin-II. *J. Biol. Chem.* 258:6011-6014.
- Kuznicki, J., G. P. Cote, B. Bowers, and E. D. Korn. 1985. Filament formation and actin-activated ATPase activity are abolished by proteolytic removal of a small peptide from the tip of the tail of the heavy chain of *Acanthamoeba* myosin-II. *J. Biol. Chem.* 260:1967-1972.
- Margossian, S. S., and W. F. Stafford. 1982. Calcium-induced dimerization of troponin-C. *J. Biol. Chem.* 257:1160-1165.
- Niederman, R., and T. D. Pollard. 1975. Human platelet myosin. II. In vitro assembly of myosin and structure of myosin filaments. *J. Cell Biol.* 67:72-92.
- Pollard, T. D. 1982. Structure and polymerization of *Acanthamoeba* myosin-II filaments. *J. Cell Biol.* 95:816-825.
- Pollard, T. D., W. F. Stafford, and M. E. Porter. 1978. Characterization of a second myosin from *Acanthamoeba castellanii*. *J. Biol. Chem.* 253:4798-4808.
- Reisler, E., S. Craig, and S. George. 1980. Myosin minifilaments. *J. Mol. Biol.* 143:129-145.
- Reisler, E., P. Cheung, C. Oriol-Audit, and J. A. Lake. 1982. Growth of synthetic myosin filaments from myosin minifilaments. *Biochemistry.* 21:701-707.
- Reisler, E., P. Cheung, and N. Borochof. 1986. Macromolecular assemblies of myosin. *Biophys. J.* 49:335-342.
- Richards, E. G., D. Teller, and H. K. Schachman. 1971. Alignment of Schlieren and Rayleigh optical systems in the ultracentrifuge. I. Focusing of the camera and cylindrical lenses. *Anal. Biochem.* 41:189-214.
- Richards, E. G., J. Bell-Clark, M. Kirschner, A. Rosenthal, and H. K. Schachman. 1972. Alignment of Schlieren and Rayleigh optical systems in the ultracentrifuge. II. Design, construction, and placement of Rayleigh mask. *Anal. Biochem.* 46:295-331.
- Roark, D. E., and D. A. Yphantis. 1969. Studies of self-associating systems by equilibrium ultracentrifugation. *Ann. NY Acad. Sci.* 164:245-278.
- Sinard, J. H., and T. D. Pollard. 1989. The effect of heavy chain phosphorylation and solution conditions on the assembly of *Acanthamoeba* myosin-II. *Cell Biol.* 109:1535-1546.
- Sophianopoulos, A. J., and K. E. Van Holde. 1964. Physical studies of muramidase (lysozyme). II. pH-dependent dimerization. *J. Biol. Chem.* 239:2516-2524.
- Stafford, W. F. 1978. An externally adjustable motor-driven Rayleigh slit assembly for the analytical ultracentrifuge. *Anal. Biochem.* 88:104-108.
- Stewart, P. R., and J. A. Spudich. 1979. Structural states of *Dictyostelium* myosin. *J. Supramol. Struct.* 12:1-14.
- Teller, D. C. 1973. Characterization of proteins by sedimentation equilibrium in the analytical ultracentrifuge. *Methods Enzymol.* 27:346-441.
- Trybus, K. M., and S. Lowey. 1985. Mechanism of smooth muscle myosin phosphorylation. *J. Biol. Chem.* 260:15988-15995.
- Trybus, K. M., and S. Lowey. 1987. Assembly of smooth muscle myosin minifilaments: effects of phosphorylation and nucleotide binding. *J. Cell Biol.* 105:3007-3019.
- Wijmenga, S. S., M. A. L. Atkinson, D. Ray, and E. D. Korn. 1987. Electric birefringence study of the solution structure of chymotrypsin-cleaved *Acanthamoeba* myosin-II. *J. Biol. Chem.* 262:15803-15808.
- Yphantis, D. A. 1964. Equilibrium ultracentrifugation of dilute solutions. *Biochemistry.* 3:297-317.